Finite Elements in Analysis and Design 45 (2009) 238 – 250

Contents lists available at ScienceDirect

Finite Elements in Analysis and Design

journal homepage: www.elsevier.com/locate/finel

A discontinuous enrichment method for the finite element solution of high Péclet advection–diffusion problems

Irina Kalashnikova[a,*], Charbel Farhat[a,b,c], Radek Tezaur[c]

[a]Institute for Computational and Mathematical Engineering (ICME), Stanford University, Stanford, CA 94305, USA
[b]Department of Aeronautics and Astronautics, Stanford University, Stanford, CA 94305, USA
[c]Department of Mechanical Engineering, Stanford University, Stanford, CA 94305, USA

ARTICLE INFO

Article history:
Received 2 September 2008
Accepted 13 October 2008
Available online 5 December 2008

Keywords:
Advection–diffusion
Boundary layer
Discontinuous enrichment method
Discontinuous Galerkin method
Finite elements
High Péclet number
Lagrange multipliers

ABSTRACT

A discontinuous enrichment method (DEM) for the efficient finite element solution of the two-dimensional advection–diffusion equation is presented. Following the general DEM, the standard Galerkin polynomial field is locally enriched with free-space solutions of the homogeneous and constant-coefficient version of the governing partial differential equation. For the advection–diffusion equation, the free-space solutions are exponential functions that exhibit a steep gradient in the advection direction. The continuity of the solution across the element boundaries is weakly enforced by a carefully discretized Lagrange multiplier field. Preliminary results for previously published benchmark problems reveal that the DEM elements proposed in this paper are significantly more competitive than their Galerkin and stabilized Galerkin counterparts, especially in advection-dominated (high Péclet number) flows. Whereas spurious oscillations are known to pollute the standard Galerkin solution unless a very fine mesh is used, the DEM solution is shown to deliver an impressive accuracy at low mesh resolution.

1. Introduction

The standard Galerkin finite element method (FEM) approximates the solution to a partial differential equation (PDE) by continuous, piecewise polynomial basis functions. FEM is quasi-optimal for elliptic boundary value problems (BVPs) in that the accuracy of the numerical solution it provides differs from that of the best approximation in the underlying finite element space by a mere constant C. Although this property assures good performance at any mesh resolution for the Laplace operator, the standard Galerkin FEM can be prohibitively expensive for many other BVPs, particularly those governed by operators that are prone to losing ellipticity. The solutions of these problems often exhibit sharp gradients or rapid oscillations, features that standard piecewise polynomial basis functions simply cannot capture unless the mesh is substantially refined or a very high order polynomial interpolant is used.

The advection–diffusion equation is among the set of equations for which the standard FEM can be inadequate. This equation describes many transport phenomena and arises in its vector form in the linearization of the Navier–Stokes equations. The asymmetric advection–diffusion operator is

$$\mathscr{L}u \equiv \underbrace{-\kappa\Delta u}_{\text{diffusion}} + \underbrace{\mathbf{a}\cdot\nabla u}_{\text{advection}} \tag{1}$$

In the context of fluid mechanics, $\mathbf{a}$ denotes the flow velocity vector; it is also often referred to as the vector of advection coefficients. In two dimensions (2D), $\mathbf{a}^{\mathrm{T}} \equiv (a_1\ a_2)$, where the superscript T designates the transpose operation. In general, $\mathbf{a}$ is a function of x and y so that $a_1(\mathbf{x}), a_2(\mathbf{x}) : \mathbb{R}^2 \to \mathbb{R}$. However, for simplicity, the scope of this paper is limited to the constant-coefficient case. The velocities a_1 and a_2 define the advection direction whose angle with the x-axis is denoted in this paper by ϕ. The quantities a_1, $a_2$and ϕ are related by

$$a_1 = |\mathbf{a}|\cos\phi, \quad a_2 = |\mathbf{a}|\sin\phi \tag{2}$$

In Eq. (1), κ denotes the diffusivity. For simplicity and without any loss of generality, this parameter is set to

$$\kappa \equiv 1 \tag{3}$$

throughout the remainder of this paper. This effectively amounts to absorbing the diffusivity into the velocity vector: $\mathbf{a} \leftarrow \mathbf{a}/\kappa$.

Associated with the advection–diffusion equation is the Péclet number, a dimensionless parameter which relates the rate of advection of a flow to its rate of diffusion. For $\kappa = 1$, the global Péclet

* Corresponding author. Tel.: +1 248 470 9203.
E-mail address: irinak@stanford.edu (I. Kalashnikova).

0168-874X/$ - see front matter © 2008 Elsevier B.V. All rights reserved.
doi:10.1016/j.finel.2008.10.009

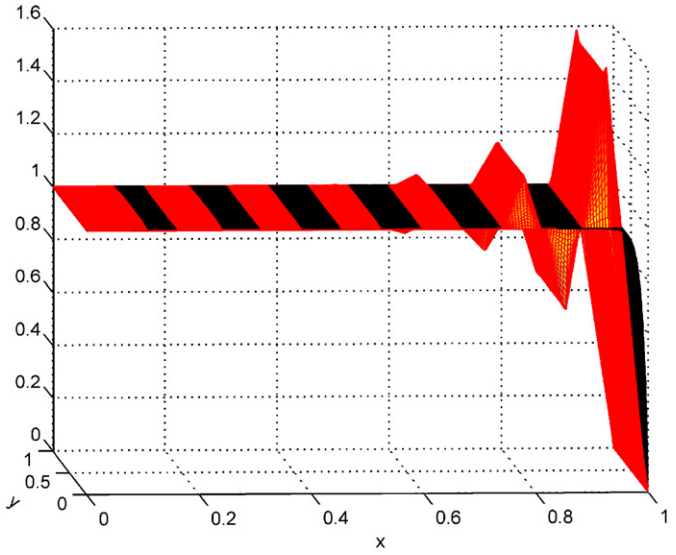

Fig. 1. Spurious oscillations in the standard Galerkin solution at high Pe number.

number on some open, bounded domain $\Omega \subset \mathbb{R}^2$ is defined as

$$Pe = \frac{\text{rate of advection}}{\text{rate of diffusion}} = \frac{l_\Omega |\mathbf{a}|}{\kappa} = l_\Omega |\mathbf{a}| = Re \cdot \begin{cases} Pr \text{ (thermal diffusion)} \\ Sc \text{ (mass diffusion)} \end{cases} \quad (4)$$

where l_Ω is a length scale characteristic of the entire domain Ω, and Re, Pr and Sc are the Reynolds, Prandtl and Schmidt numbers, respectively. For example, if Ω is an $L \times L$ square obstacle, one can naturally choose $l_\Omega = L$.

In typical applications, the magnitude of the diffusion is very small compared to the magnitude of the advection and therefore the Péclet number is high. It is well known that the solution of an advection–diffusion BVP displays sharp boundary layers when the Péclet number is high—that is, when $|\mathbf{a}|$ is large. The velocity profile rises sharply within the thin, viscous boundary layer to the more or less constant free-stream velocity away from the wall or surface boundary (black curve in Fig. 1). Therefore, the exact solution of such a BVP problem exhibits two scales: a rapidly varying fine scale in the diffusion-dominated boundary layer region, and a slowly varying coarse scale in the advection-dominated free-stream region. This multi-scale behavior challenges the effective and accurate numerical solution of the underlying BVPs. Spurious oscillations pollute the Galerkin FEM solution unless a very fine mesh is used within the boundary layer (red curve in Fig. 1). A number of different finite element approaches have been proposed for addressing this and similar challenges for other PDEs. These alternatives to the standard FEM fall roughly into two categories: those based on a modified variational formulation, and those based on a modified finite element basis.

Stabilized FEMs fall into the first category of methods identified above. Motivated by the observation that the standard Galerkin FEM produces dispersive, central-difference type approximations, the basic idea was to add to the variational formulation some numerical diffusion terms in order to stabilize the computed solution. Such methods include the streamline upwind Petrov–Galerkin (SUPG or streamline diffusion) method [1,2], Galerkin least-squares (GLS) [3,4] and the unusual stabilized finite element method (USFEM) [5,6]. More recent variants of these approaches analyze the spurious anisotropy that is inherent to the Galerkin method. Many of these variants also attempt to improve the stabilization by incorporating into it error estimators [7] or deriving stability parameters that take into account the direction of the flow [8]. In all cases, stabilized FEM have relied on the same polynomial basis functions as those employed by the standard FEM.

In contrast with the first category of alternatives to the standard FEM, the second category is essentially based on non-standard finite element bases. In some cases, this has also called for modified variational formulations. Examples of such alternative methods include the method of residual-free bubbles (RFB) [9,10], the partition of unity method (PUM) [11,12] and the discontinuous enrichment method (DEM) [13–17]. Whereas RFB and PUM are continuous methods, DEM is a discontinuous one. DEM distinguishes itself from previously [18,19] as well as recently proposed [20,21] discontinuous Galerkin methods (DGMs) either by its special shape functions that are typically non-polynomial, or by the Lagrange multiplier degrees of freedom (dofs) it introduces at the element interfaces to enforce there a weak continuity of the numerical solution, or by both of these discretization ingredients.

DEM was first proposed by Farhat and co-workers in [13]. This method enriches in each element the polynomial field of the standard FEM by free-space solutions of the homogeneous, constant-coefficient version of the governing PDE. This type of enrichment has a natural potential for effectively resolving sharp gradients and rapid oscillations when these are present in the computational domain. Unlike in PUM, the enrichment in DEM is performed in an additive rather than multiplicative manner. Unlike in RFB, it is *not* constrained to vanish at the element boundaries and therefore can propagate its beneficial effect to the neighboring elements. Unlike in both PUM and RFB, the enrichment in DEM leads to a discontinuous rather than continuous approximation in which the enrichment dofs can be eliminated at the element level by static condensation. This reduces computational complexity and alleviates some of the ill-conditioning that is inherent to most enrichments. Finally, unlike in standard DGMs, a weak continuity of the solution across the element interfaces is enforced in DEM using Lagrange multipliers.

DEM has demonstrated a strong performance for acoustic scattering, wave propagation in elastic media and fluid–structure interaction problems governed by the Helmholtz equation, Navier's equations and the coupling of these equations, respectively [15–17]. The Helmholtz operator $\mathscr{L}u = -\Delta u - k^2 u$ describing, among others, acoustic vibrations in a fluid medium, tends to lose ellipticity with an increasing wave number k. Consequently, the Galerkin solution of Helmholtz problems is tainted by spurious dispersion in the upper end of the low frequency regime, and is intractable in the medium and high frequency regimes. In [15], a family of three-dimensional (3D) hexahedral DEM elements of increasing order of convergence were proposed for the solution of acoustic scattering problems in the medium frequency regime. When compared with standard high-order polynomial Galerkin elements of comparable convergence order, the DEM elements achieved the same solution accuracy using however four to eight times fewer dofs, and most importantly, *up to 60 times less CPU time* [15]. Similar impressive results were achieved by DEM for problems involving multi-scale fluid/solid interfaces [16] and elastic wave propagation [17].

The excellent performance demonstrated by DEM for acoustic scattering and wave propagation problems is the main motivation behind this work which essentially extends DEM to advection–diffusion problems. This extension is a first step towards the far more challenging step of solving the Navier–Stokes equations by DEM. To begin, the scope of the extension is limited to 2D, rectangular domains, and relatively low order DEM elements. This allows focusing on the general idea and its potential.

The remainder of this paper is organized as follows. Section 2 presents the hybrid variational formulation associated with the solution by DEM of the typical 2D advection–diffusion BVP. Section 3

focuses on the derivation and approximation of the enrichment field. Section 4 shifts the attention to the corresponding Lagrange multiplier field. Section 5 presents a discussion of DEM element design for the advection-diffusion problem and specifies a low order family of such elements. The performance of this family of DEM elements is assessed in Section 6 on several previously published benchmark problems, and conclusions are offered in Section 7.

2. Theoretical framework of DEM

Let $\Omega \subset \mathbb{R}^2$ be an open bounded domain with a sufficiently smooth boundary $\Gamma \equiv \partial\Omega$. As a canonical example, consider the following all-Dirichlet BVP for the 2D advection–diffusion equation in its strong form (S).

$$(S): \begin{cases} \text{Find } u: \bar{\Omega} \to \mathbb{R} \text{ such that } u \in H^1(\Omega) \text{ and} \\ \mathscr{L}u \equiv -\Delta u + \mathbf{a}\cdot\nabla u = f \quad \text{in } \Omega \\ u = g \quad \text{on } \Gamma \end{cases} \tag{5}$$

Here, $f: \Omega \to \mathbb{R}$ and $g: \Gamma \to \mathbb{R}$ are given functions.

Partition Ω into n_{el} non-overlapping element domains Ω^e, each having a boundary Γ^e, for $e = 1, 2, \ldots, n_{el}$, as shown in Fig. 2. This can be written mathematically as

$$\overline{\Omega} = \overline{\bigcup_{e=1}^{n_{el}} \Omega^e} \quad \text{with} \quad \bigcap_{e=1}^{n_{el}} \Omega^e = \emptyset \tag{6}$$

The union of element interiors and element boundaries are denoted by $\tilde{\Omega}$ and $\tilde{\Gamma}$, respectively,

$$\tilde{\Omega} = \bigcup_{e=1}^{n_{el}} \Omega^e, \quad \tilde{\Gamma} = \bigcup_{e=1}^{n_{el}} \Gamma^e \tag{7}$$

The set of element interfaces (or interior element boundaries) is denoted by

$$\Gamma_{\text{int}} = \tilde{\Gamma} \backslash \Gamma \tag{8}$$

and the intersection between two adjacent element boundaries Γ^e and $\Gamma^{e'}$ is denoted by

$$\Gamma^{e,e'} = \Gamma^e \cap \Gamma^{e'} \tag{9}$$

2.1. Hybrid variational formulation

The formulation of DEM is obtained by rewriting the strong form (S) of BVP (5) in its weak variational form. To this effect, two functional spaces are introduced

$$\mathscr{V} \equiv \{v \in L^2(\tilde{\Omega}) : v|_{\Omega^e} \in H^1(\Omega^e)\} \tag{10}$$

$$\mathscr{W} = \Pi_e \Pi_{e'<e} H^{-1/2}(\Gamma^{e,e'}) \times H^{-1/2}(\Gamma) \tag{11}$$

$\mathscr{V}$ is a space of element approximations of the solution and $\mathscr{W}$ is a space of Lagrange multipliers. The space $\mathscr{W}$ is needed to enforce the continuity of the solution as the element approximations in $\mathscr{V}$ are allowed to be discontinuous across the element boundaries. The weak form of BVP (5) is obtained first by multiplying the first equation by a test function $v \in \mathscr{V}$ and integrating the diffusion term by parts. This can be written as

$$\int_\Omega (-\Delta u + \mathbf{a}\cdot\nabla u) v \, \mathrm{d}\Omega = -\int_\Gamma \underbrace{(\nabla u \cdot \mathbf{n})}_{\equiv \mathscr{L}_b u} v \, \mathrm{d}\Gamma + \int_\Omega (\nabla u \cdot \nabla v + \mathbf{a}\cdot\nabla u v) \, \mathrm{d}\Omega \tag{12}$$

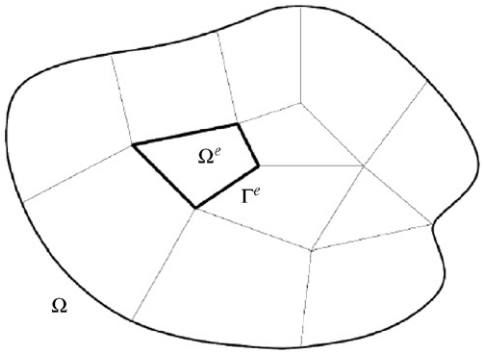

Fig. 2. Partition of domain Ω into elements Ω^e.

Here, $\mathscr{L}_b$ is the boundary operator corresponding to $\mathscr{L}$. Constraining the solution to remain continuous across the element interfaces leads to the following weak hybrid variational formulation:

$$(W): \begin{cases} \text{Find } (u, \lambda) \in \mathscr{V} \times \mathscr{W} \text{ such that} \\ a(v,u) + b(\lambda, v) = r(v) \quad \forall v \in \mathscr{V} \\ b(\mu, u) = -r_d(\mu) \quad \forall \mu \in \mathscr{W} \end{cases} \tag{13}$$

where $a(\cdot,\cdot)$ and $b(\cdot,\cdot)$ are bilinear forms on $\mathscr{V} \times \mathscr{V}$ and $\mathscr{W} \times \mathscr{V}$, respectively, and are given by

$$a(v,u) \equiv (\nabla v + v\mathbf{a}, \nabla u)_{\tilde{\Omega}} = \int_{\tilde{\Omega}} (\nabla v \cdot \nabla u + v\mathbf{a}\cdot\nabla u) \, \mathrm{d}\Omega \tag{14}$$

$$b(\lambda, v) \equiv \sum_e \sum_{e'<e} \int_{\Gamma^{e,e'}} \lambda (v_{e'} - v_e) \, \mathrm{d}\Gamma + \int_\Gamma \lambda v \, \mathrm{d}\Gamma \tag{15}$$

and $r(v)$ and $r_d(\mu)$ (d for "Dirichlet") are the following linear forms:

$$r(v) \equiv (f, v) = \int_\Omega f v \, \mathrm{d}\Omega \tag{16}$$

$$r_d(\mu) \equiv \int_\Gamma \mu g \, \mathrm{d}\Gamma \tag{17}$$

In (14) and (16), $(\cdot,\cdot)$ denotes the usual L^2 inner product over Ω; in (15), $v_e \equiv v|_{\Omega^e}$. Note that the bilinear form $a(\cdot,\cdot)$ in (14) is *not* symmetric ($a(v,u) \neq a(u,v)$) for the advection–diffusion operator due to the presence of the first order advection term.

Denoting the jump at an element boundary by $[\cdot]$, the Euler–Lagrange equations corresponding to (W) are

$$\begin{aligned} &\mathscr{L}u \equiv -\Delta u + \mathbf{a}\cdot\nabla u = f \quad \text{in } \tilde{\Omega} \\ &[\mathbf{u}] = 0 \quad \text{on } \Gamma_{int} \\ &u = g \quad \text{on } \Gamma \\ &\lambda = \mathscr{L}_b u = \nabla u \cdot \mathbf{n} \quad \text{on } \tilde{\Gamma} \end{aligned} \tag{18}$$

The last of Eqs. (18) provides an interpretation of the Lagrange multiplier field: since for this problem the boundary operator $\mathscr{L}_b$ corresponding to $\mathscr{L}$ is the normal derivative of the solution (see (12)), the Lagrange multiplier field is the normal derivative of the solution at the element boundaries.

2.2. Approximation spaces

Let $\mathscr{V}^h \subset \mathscr{V}$ and $\mathscr{W}^h \subset \mathscr{W}$ be the finite dimensional versions of the solution approximation and Lagrange multiplier spaces defined in (10) and (11). In the classical Galerkin FEM, the trial functions are

Table 1
Approximation spaces for DGM and true DEM elements

	$\mathscr{V}^h$	u^h
DGM	$\mathscr{V}^E$	u^E
DEM	$\mathscr{V}^P \oplus (\mathscr{V}^E \setminus \mathscr{V}^P)$	$u^P + u^E$

continuous piecewise polynomials within each element Ω^e—that is, $u^h = u^P$ with

$$u^P \in \mathscr{V}^P \subset P_n(x,y) \subset H^1(\Omega) \tag{19}$$

where

$$P_n(x,y) \equiv \left\{ p \in H^1(\Omega^e) : p(x,y) = \sum_{i=0}^{n} a_i x^i y^i, (x,y) \in \Omega^e, a_i \in \mathbb{R} \right\} \tag{20}$$

is the usual polynomial interpolation space. In DEM, this standard polynomial field is "enriched" with the free-space solutions of the homogeneous form of the governing PDE that are not already represented in $\mathscr{V}^P$. This enrichment field is denoted by u^E and the space it belongs to is denoted by $\mathscr{V}^E$, with

$$\mathscr{V}^E \subset \{u^E \in L^2(\mathbb{R}^2) : \mathscr{L}u^E = -\Delta u^E + \mathbf{a} \cdot \nabla u^E = 0\} \tag{21}$$

Since the enrichment functions are employed on an element level, the free-space solutions of the homogeneous *constant*-coefficient version of the governing PDE can be obtained with little difficulty using standard PDE techniques—for example, the method of separation of variables (Section 3).

The basic idea of DEM is to seek an approximate solution $(u^h, \lambda^h) \subset \mathscr{V}^h \times \mathscr{W}^h$ to the hybrid variational problem (13) where the primal unknown u^h has one of the two forms given in Table 1. Hence, two varieties of DEM can be defined: a true or "full" DEM, and an enrichment-only DEM referred to in the remainder of this paper as "DGM".

In the case of true DEM elements, the solution space $\mathscr{V}^h$ is constructed as a direct sum of $\mathscr{V}^P$ and $\mathscr{V}^E$. This splitting of the approximation into polynomials and enrichment functions can be viewed as a decomposition of the numerical solution into coarse (polynomial) scales and fine (enrichment) scales. Since the enrichment field contains free-space solutions of the underlying equation to be solved, it may entirely capture the homogeneous solutions rather than merely enhance the polynomial field. In fact, as will be shown in Section 6, for homogeneous BVPs u^P contributes little, if at all, to the computed solution. This premise motivates the construction of enrichment-only DGM elements in which the contribution of the standard polynomial field is dropped from the approximation entirely, resulting in improved computational efficiency without any loss of accuracy [14].

2.3. Galerkin formulation and implementation

Assuming the more general case of the full DEM and substituting the approximation u^h (second row of Table 1) into the weak form (13) results in the following discrete Galerkin problem:

$$(G): \begin{cases} \text{Find } (u^h, \lambda^h) \in \mathscr{V}^h \times \mathscr{W}^h \text{ such that} \\ a(v^P, u^P) + a(v^P, u^E) + b(\lambda^h, v^P) = r(v^P) \\ a(v^E, u^P) + a(v^E, u^E) + b(\lambda^h, v^E) = r(v^E) \\ b(\mu^h, v^P) + b(\mu^h, v^E) = -r_d(\mu^h) \\ \text{holds } \forall (v^h, \mu^h) \in \mathscr{V}^h \times \mathscr{W}^h \end{cases} \tag{22}$$

The above system of Galerkin equations (G) gives rise to the element matrix equation

$$\underbrace{\begin{pmatrix} \mathbf{k}^{PP} & \mathbf{k}^{PE} & \mathbf{k}^{PC} \\ \mathbf{k}^{EP} & \mathbf{k}^{EE} & \mathbf{k}^{EC} \\ \mathbf{k}^{CP} & \mathbf{k}^{CE} & \mathbf{0} \end{pmatrix}}_{\equiv \mathbf{k}^e} \begin{pmatrix} \mathbf{u}^P \\ \mathbf{u}^E \\ \boldsymbol{\lambda} \end{pmatrix} = \underbrace{\begin{pmatrix} \mathbf{r}^P \\ \mathbf{r}^E \\ \mathbf{r}^C \end{pmatrix}}_{\equiv \mathbf{r}^e} \tag{23}$$

where $\mathbf{u}^P$, $\mathbf{u}^E$ and $\boldsymbol{\lambda}$ are vectors containing the local dofs u^P, u^E and λ^h, respectively[1]; the superscript e designates the element domain and the superscript C designates the continuity constraints enforced by the Lagrange multipliers. The correspondence between the matrices and the Galerkin equations is obtained by comparing (22) and (23). Note that $\mathbf{k}^{EP} \neq \mathbf{k}^{PE^{\mathrm{T}}}$ as a result of the asymmetry of the bilinear form $a(\cdot,\cdot)$ for the advection–diffusion operator. In the case of a DGM implementation, $\mathbf{k}^{PP}, \mathbf{k}^{PE}, \mathbf{k}^{PC}, \mathbf{k}^{EP}, \mathbf{k}^{CP}, \mathbf{r}^P = \{\emptyset\}$ (that is, they are empty and can be omitted) and therefore the three-by-three block system (23) reduces to a two-by-two block system.

Due to the discontinuous nature of $\mathscr{V}^E$, u^E can be eliminated at the element level by a static condensation. For a full DEM element, taking the Schur complement of the second equation in (23) and substituting this expression into the first and third equations leads to the following (local) statically condensed system:

$$\underbrace{\begin{pmatrix} \tilde{\mathbf{k}}^{PP} & \tilde{\mathbf{k}}^{PC} \\ \tilde{\mathbf{k}}^{CP} & \tilde{\mathbf{k}}^{CC} \end{pmatrix}}_{\equiv \tilde{\mathbf{k}}^e} \begin{pmatrix} \mathbf{u}^P \\ \boldsymbol{\lambda} \end{pmatrix} = \underbrace{\begin{pmatrix} \tilde{\mathbf{r}}^P \\ \tilde{\mathbf{r}}^C \end{pmatrix}}_{\equiv \tilde{\mathbf{r}}^e} \tag{24}$$

where

$$\tilde{\mathbf{k}}^{PP} = \mathbf{k}^{PP} - \mathbf{k}^{PE}(\mathbf{k}^{EE})^{-1}\mathbf{k}^{EP} \tag{25}$$

$$\tilde{\mathbf{k}}^{PC} = \mathbf{k}^{PC} - \mathbf{k}^{PE}(\mathbf{k}^{EE})^{-1}\mathbf{k}^{EC} \tag{26}$$

$$\tilde{\mathbf{k}}^{CP} = \mathbf{k}^{CP} - \mathbf{k}^{CE}(\mathbf{k}^{EE})^{-1}\mathbf{k}^{EP} \tag{27}$$

$$\tilde{\mathbf{k}}^{CC} = -\mathbf{k}^{CE}(\mathbf{k}^{EE})^{-1}\mathbf{k}^{EC} \tag{28}$$

and

$$\tilde{\mathbf{r}}^P = \mathbf{r}^P - \mathbf{k}^{PE}(\mathbf{k}^{EE})^{-1}\mathbf{r}^E \tag{29}$$

$$\tilde{\mathbf{r}}^C = \mathbf{r}^C - \mathbf{k}^{CE}(\mathbf{k}^{EE})^{-1}\mathbf{r}^E \tag{30}$$

In the case of a DGM element, there is no polynomial field and therefore $\tilde{\mathbf{k}}^{PP}, \tilde{\mathbf{k}}^{PC}, \tilde{\mathbf{k}}^{CP}, \tilde{\mathbf{r}}^P = \{\emptyset\}$. Since $\tilde{\mathbf{k}}^{CC}$ reduces to $\tilde{\mathbf{k}}^{CC} = -\mathbf{k}^{CE}(\mathbf{k}^{EE})^{-1}\mathbf{k}^{EC}$, the statically condensed system for a DGM element simply is

$$\underbrace{-\mathbf{k}^{CE}(\mathbf{k}^{EE})^{-1}\mathbf{k}^{EC}}_{=\mathbf{k}^e=\tilde{\mathbf{k}}^{CC}} \boldsymbol{\lambda} = \underbrace{\mathbf{r}^C - \mathbf{k}^{CE}(\mathbf{k}^{EE})^{-1}\mathbf{r}^E}_{=\tilde{\mathbf{r}}^e=\tilde{\mathbf{r}}^C} \tag{31}$$

Algorithm 1 Element-level static condensation algorithm.

Compute the entries of the element matrices in (23) using (22).
Compute the local Schur complements in (25)–(30).
Assemble the global interface problem (24).
Solve for the vector λ (and the vector $\mathbf{u}^P$, if applicable, i.e., in the case of the full DEM).
for each element Ω^e, $e = 1, \ldots, n_{el}$ **do**
Compute $\mathbf{u}^E$ as a post-processing step within Ω^e as follows:

$$\mathbf{k}^{EE}\mathbf{u}^E = \mathbf{r}^E - \mathbf{k}^{EP}\mathbf{u}^P - \mathbf{k}^{EC}\boldsymbol{\lambda} \tag{32}$$

(with $\mathbf{k}^{EP} = \{\emptyset\}$ in the case of a DGM element.)
end for

[1] The discussion of the Lagrange multiplier approximations λ^h is deferred until Section 4 (Eq. (50)).

Eqs. (24) and (31) give rise either to a $u^P - \lambda$ formulation for the full DEM approximation, or simply to a λ-formulation for its DGM variant. The global condensed system is obtained from an assembly of the statically condensed element arrays $\tilde{\mathbf{k}}^e$ and $\tilde{\mathbf{r}}^e$. From this system, the Lagrange multiplier dofs, and, when applicable, the polynomial dofs, are solved for, after which the enrichment dofs are computed by means of a post-processing step local to each element. The key steps of this implementation are summarized in Algorithm 1.

2.4. Important remark on computational complexity

The cost of solving the global interface problem (24) is not directly determined by the dimension of $\mathscr{V}^E$. Instead, it depends on the total number of Lagrange multiplier dofs[2]— that is, on $\dim \mathscr{W}^h$. This property is a result of the element-level static condensation which is enabled by the discontinuous nature of the approximation of the solution. As discussed in Section 4 of this paper, the Babuška–Brezzi *inf–sup* condition which must be satisfied to ensure that the global interface problem is non-singular limits the total number of Lagrange multiplier dofs as follows:

$$\begin{Bmatrix} \#\text{ of enrichment} \\ \text{equations} \end{Bmatrix} \leqslant \begin{Bmatrix} \#\text{Lagrange multiplier} \\ \text{constraint equations} \end{Bmatrix} \tag{33}$$

The computational complexity of specific DGM and DEM elements is discussed in Section 5 of this paper.

3. Enrichment basis for the 2D advection–diffusion equation

To obtain the enrichment basis u^E for the 2D advection–diffusion equation, the equation $\mathscr{L}u^E = -\Delta u^E + \mathbf{a}\cdot\nabla u^E = 0$ is solved assuming constant advection coefficients $\mathbf{a}^{\mathrm{T}} = (a_1 a_2) \in \mathbb{R}^2$. One way to achieve this objective is to use the technique of separation of variables assume a solution of the form

$$u^E(x,y) = F(x)G(y) \tag{34}$$

for some C^2 functions $F, G : \mathbb{R} \to \mathbb{R}$, and determine F and G such that $\mathscr{L}u^E = 0$ is satisfied. Doing so gives

$$F_k(x) = \begin{cases} e^{a_1 x/2}\left[A\exp\left(\frac{\sqrt{\alpha^2}}{2}x\right) + B\exp\left(-\frac{\sqrt{\alpha^2}}{2}x\right)\right] & \text{if } k \leqslant \frac{a_1^2}{4} \\ e^{a_1 x/2}\left[A\cos\left(\frac{\sqrt{-\alpha^2}}{2}x\right) + B\sin\left(\frac{\sqrt{-\alpha^2}}{2}x\right)\right] & \text{if } k > \frac{a_1^2}{4} \end{cases} \tag{35}$$

$$G_k(y) = \begin{cases} e^{a_2 y/2}\left[C\exp\left(\frac{\sqrt{\beta^2}}{2}y\right) + D\exp\left(\frac{-\sqrt{\beta^2}}{2}y\right)\right] & \text{if } k \geqslant -\frac{a_2^2}{4} \\ e^{a_2 y/2}\left[C\cos\left(\frac{\sqrt{-\beta^2}}{2}y\right) + D\sin\left(\frac{\sqrt{-\beta^2}}{2}y\right)\right] & \text{if } k < -\frac{a_2^2}{4} \end{cases} \tag{36}$$

with

$$\alpha^2 \equiv a_1^2 - 4k \tag{37}$$

$$\beta^2 \equiv a_2^2 + 4k \tag{38}$$

Here, A, B, C, D and k are real constants. The form of the solution depends on the value of the separation of variables constant k relative to the given advection velocities a_1 and a_2. Results (35) and (36) imply that the solution can take on one of three forms that are summarized in Table 2.

In the first case, the enrichment function u^E is a rapidly rising or falling exponentially in both x and y directions. In the second and third cases, the enrichment is oscillatory in one direction. Note however that unless there is a trigonometric source in Eq. (5), the solutions of these BVPs do *not* exhibit an oscillatory behavior; they exhibit however sharp *exponential* boundary layers in which the velocity profile rises or falls sharply, much like the functions in the first case of Table 2. Because of this observation, only the enrichment functions that are exponential in both x and y are considered in this work so that

Table 2
Forms of the free-space solution u^E to $\mathscr{L}u^E = 0$

k	$F_k(x)$	$G_k(y)$
$\in \left[-\frac{a_2^2}{4}, \frac{a_1^2}{4}\right]$	Exponential	Exponential
$\in \left(-\infty, -\frac{a_2^2}{4}\right)$	Exponential	Trigonometric
$\in \left(\frac{a_1^2}{4}, \infty\right)$	Trigonometric	Exponential

$$u^E(x,y) = e^{(a_1/2 \pm \alpha/2)x} e^{(a_2/2 \pm \beta/2)y} \tag{39}$$

Enrichment basis functions can now be generated by varying the signs in (39) and the constant k in (37) and (38).

Remark 1. An upshot of the exponential solutions of $\mathscr{L}u^E = 0$ in the DEM basis is that, assuming a simple enough element geometry, all the components of the element matrices (23) can be computed analytically, as exponentials are easy to integrate and differentiate. One can therefore avoid the quadrature error that would be introduced into the approximation if these integrals were to be computed numerically.

While expression (39) is correct mathematically and solves $\mathscr{L}u^E = 0$ for any choice of $k \in \mathbb{R}$, there is a practical issue that is worth addressing: it is unclear how the parameter k should be selected to generate a particular enrichment basis, since this parameter can take on *any* real value from $-\infty$ to ∞. To this effect, it is recalled here that when DEM was tailored to the 2D Helmholtz equation $-\Delta u - k^2 u = 0$ in [14], the enrichment space $\mathscr{V}^E$ consisted of a superposition of 2D plane waves $u^E|_{\Omega^e} = e^{ikx\cos\theta_p} e^{iky\sin\theta_p}$, where $i = \sqrt{-1}$, propagating in directions $\theta_p \in [0, 2\pi)$. The fact that the basis functions for the Helmholtz equation were specified by an angle proved to be very convenient as it made possible the systematic design of DEM elements of arbitrary orders. Indeed, to design an element of order n^E, one simply selected n^E plane waves propagating in n^E different directions.

Guided by DEM for the Helmholtz equation, an expression for u^E is sought after here in which the constant k is replaced by some angle parameter. To rewrite (39) in terms of a similar angle parameter, observe that

$$\alpha^2 + \beta^2 = a_1^2 + a_2^2 \tag{40}$$

where α^2 and β^2 were defined in Eqs. (37) and (38) respectively. Relation (40) suggests the following parameterizations:

$$\alpha \equiv |\mathbf{a}|\cos\theta_i, \quad \beta \equiv |\mathbf{a}|\sin\theta_i \tag{41}$$

for some angle $\theta_i \in [0, 2\pi)$, where

$$|\mathbf{a}| = \sqrt{a_1^2 + a_2^2} \tag{42}$$

With this notation in place, Eq. (39) becomes

$$u^E(\mathbf{x};\theta_i) = e^{((a_1 + |\mathbf{a}|\cos\theta_i)/2)x} e^{((a_2 + |\mathbf{a}|\sin\theta_i)/2)y} \tag{43}$$

[2] It also depends on the sparsity pattern of the system matrices (see Section 5.1, Table 3).

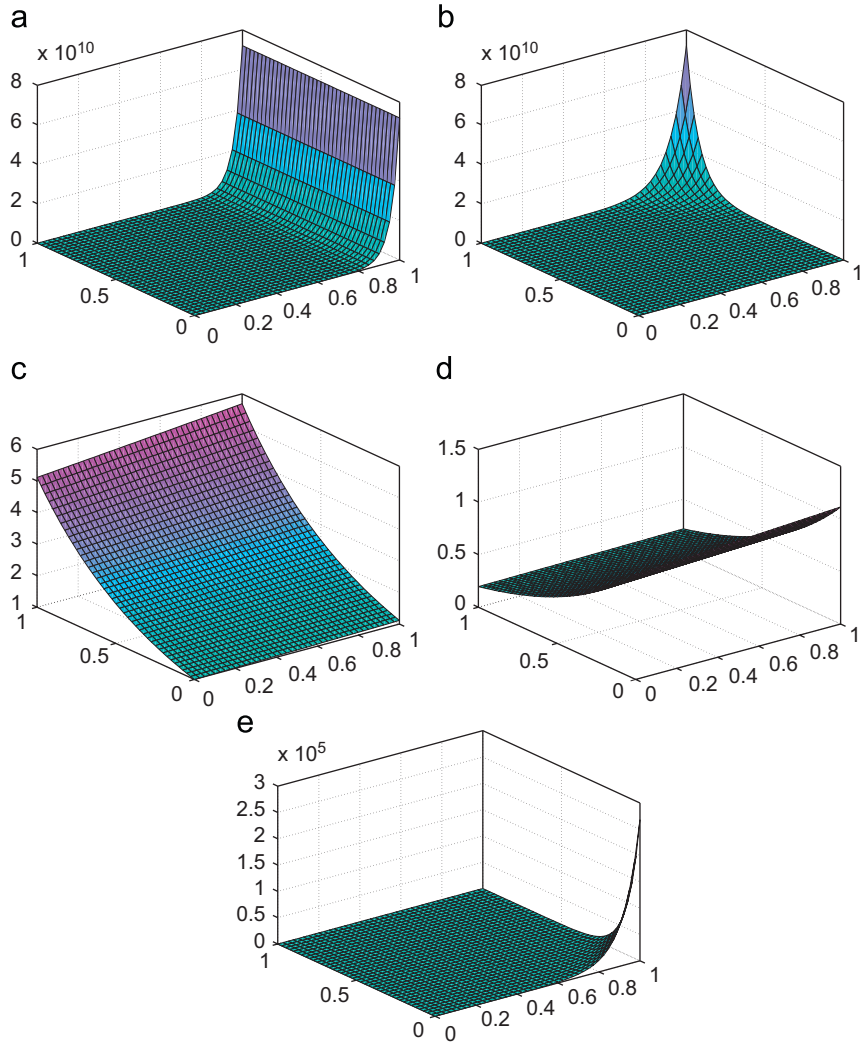

Fig. 3. Plots of enrichment functions $u^E(\mathbf{x};\theta_i)$ for several values of θ_i ($a_1=25$, $a_2=0$). (a) $\theta_i=0$. (b) $\theta_i=\pi/2$. (c) $\theta_i=23\pi/24$. (d) $\theta_i=25\pi/24$. (e) $\theta_i=3\pi/2$.

The enrichment space $\mathscr{V}^E$ can now be written as the following superposition of the 2D exponential enrichment functions (43):

$$\mathscr{V}^E \equiv \left\{ u^E \in L^2(\tilde{\Omega}) : u|^E_{\Omega^e}(x,y) = \sum_{i=1}^{n^E} u_i \mathrm{e}^{((a_1+|\mathbf{a}|\cos\theta_i)/2)(x-x_r^e)} \mathrm{e}^{((a_2+|\mathbf{a}|\sin\theta_i)/2)(y-y_r^e)}, \quad 0 \leqslant \theta_i < 2\pi, \quad u_i \in \mathbb{R} \right\} \tag{44}$$

where n^E is the number of enrichment functions (the dimension of the space $\mathscr{V}^E$) and is selected *a priori* in this preliminary work.

Remark 2. In (44), $\mathbf{x}_r^e = (x_r^e\ y_r^e)^{\mathrm{T}}$ is an arbitrary reference point assigned to element Ω^e. This reference point has the practical purpose of scaling the enrichment functions to prevent them from evaluating to a very large number on a finite precision arithmetic machine.

The natural interpretation of the angles θ_i is that they are flow directions. Not only does this interpretation fit in nicely with the problem at hand, it also facilitates the design and implementation of DGM/DEM elements of arbitrary orders. Indeed, to design an element of order n^E, one simply selects n^E angles $\theta_i \in [0, 2\pi)$. Each of these angles specifies a basis function of the form (43) (see Section 5). The set of angles $\{\theta_i\}$ specifying an enrichment basis is denoted as

$$\Theta \equiv \{\text{set of angles } \{\theta_i\} \text{ defining } \mathscr{V}^E\} \tag{45}$$

A strategy for constructing a space $\mathscr{V}^E$ of dimension n^E is to select the angles $\{\theta_i\} \in \Theta$ such that the enrichment functions they specify "slope"—that is, exhibit a sharp gradient—in n^E different directions. Fig. 3 shows plots of the enrichment basis functions for several angles θ_i.

Of particular interest is the relationship between θ_i and the advection direction ϕ (2) implied by the advection coefficients a_1 and a_2 (Fig. 4). Setting $\theta_i = \phi$ in (43), one finds that $u^E(\mathbf{x}\phi)$ simplifies to

$$u^E(\mathbf{x};\phi) = \mathrm{e}^{a_1(x-x_r^e)} \mathrm{e}^{a_2(y-y_r^e)} \tag{46}$$

Function (46) has the property that

$$\nabla u^E(\mathbf{x};\phi) = \mathbf{a} u^E(\mathbf{x};\phi) \tag{47}$$

The gradient of a function points in the direction in which that function changes most rapidly; therefore (47) implies that the enrichment function specified by $\theta_i = \phi$ rises most rapidly precisely in the

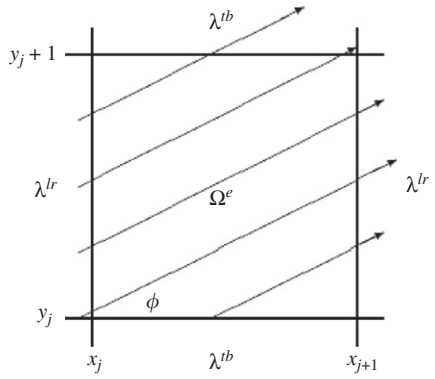

Fig. 4. Flow at an angle ϕ over $\Omega^e = (x_j, x_{j+1}) \times (y_j, y_{j+1})$.

direction of the advection ϕ. There is therefore the motivation to always include $\theta_i = \phi$ in the set Θ specifying the enrichment basis of a DGM or DEM element designed to solve a problem with advection velocities a_1 and a_2. This idea is explored further in Sections 5 and 6.

Remark 3. Since a constant is a free-space solution of the advection–diffusion equation, it should be included in the set of enrichment functions for a DGM element. A convenient property of the basis (43) is that one can generate the constant function simply by choosing one of the angles $\theta_i \in \Theta$ as $\theta_i = \phi - \pi$ shown as follows:

$$u^E(\mathbf{x}; \phi - \pi) = \text{const} \tag{48}$$

4. Approximation of the Lagrange multipliers

As stated earlier, the scope of this paper is limited for simplicity to rectangular domains. For the upcoming analysis, assume

$$\Omega = (0, L) \times (0, L) \subset \mathbb{R}^2, \quad L > 0 \tag{49}$$

and consider a partition of Ω into a uniform $n \times n$ mesh of $n_{el} = n^2$ square elements $\{\Omega^e\}$.

Attention is now turned to how to approximate the Lagrange multiplier field on $\Gamma^{e,e'}$ for $e, e' \in \{1, 2, \ldots, n_{el}\}$.

An extensive survey of techniques for discretizing a Lagrange multiplier field of a form similar to that considered in this work can be found in [22, Section 3.3]. Most, if not all, of the techniques and theoretical results established so far are for standard polynomial approximations of the solution u^h. Extending these ideas to the case of exponential approximations u^E is not a straightforward task.

The last of Eqs. (18) suggests choosing

$$\lambda^h \approx \nabla u_e^E \cdot \mathbf{n}^e = -\nabla u_{e'}^E \cdot \mathbf{n}^{e'} \quad \text{on } \Gamma^{e,e'} \tag{50}$$

as an approximation of the Lagrange multiplier along the edge $\Gamma^{e,e'}$ between two adjacent elements Ω^e and $\Omega^{e'}$. Here, $\mathbf{n}^e$ and $\mathbf{n}^{e'}$ are outward unit normals to Ω^e and $\Omega^{e'}$, respectively, and the $\approx$ symbol emphasizes that λ^h is to be approximated within the space of the normal derivatives of the functions contained in $\mathscr{V}^E$ (44) and not as the straightforward normal derivative of u_e^E.

Before computing the Lagrange multiplier approximation using (50) and the enrichment basis derived in Section 3, there is a key issue that needs to be addressed, namely, the stability of the mixed hybrid formulation (13). Recall from Section 2.4 that the well-known Babuška–Brezzi *inf–sup* condition must be verified for the discrete, finite dimensional problem (23). The outcome of this condition can be expected to relate the dimension of the space of Lagrange multipliers $\mathscr{W}^h$ to the dimension of the space of enrichment functions $\mathscr{V}^E$. The literature [22] suggests that a necessary condition for generating a non-singular global interface problem resulting from the assembly of matrices (24) is to limit the total number of constraint equations enforced by the Lagrange multipliers to the total number of enrichment equations—that is, to follow guideline (33). Given a uniform mesh of square elements, this condition translates to a bound on the number of Lagrange multipliers per edge, which is derived below. Introducing

$$n^\lambda = \#\text{ Lagrange multipliers per edge of an element} \tag{51}$$

and assuming an $n \times n$ mesh, there are $2n(n+1)$ element boundaries (including the exterior boundary Γ). It follows that in this case, there is a total of $2n(n+1)n^\lambda$ Lagrange multiplier dofs. Since

$$\begin{aligned} n_{eq} &= \text{total \# of enrichment equations} \\ &= \dim \text{ of the global matrix } \mathbf{K}^{EE} \\ &= n^2 n^E \end{aligned} \tag{52}$$

ensuring that condition (33) holds amounts to requiring

$$2(n+1)nn^\lambda \leqslant n_{eq} = n^2 n^E \tag{53}$$

or, asymptotically,

$$n^\lambda \leqslant \frac{n^E}{2} \tag{54}$$

almost everywhere in a regular mesh.

Remark 4. Bound (54) is a necessary, but in general *not* a sufficient, condition for ensuring that a non-singular global interface problem arises in the application of the DEM on a uniform mesh of square elements. In practice, fewer than $n^\lambda = n^E/2$ Lagrange multipliers per edge will be used. Numerical tests show that the general rule of thumb is to limit

$$n^\lambda = \left\lfloor \frac{n^E}{4} \right\rfloor \tag{55}$$

where $\lfloor x \rfloor \equiv \max\{n \in \mathbb{Z} | n \leqslant x\}$ for any $x \in \mathbb{R}$.

Next, the Lagrange multiplier approximation is derived using (50) and the enrichment functions (43). Let

$$\Theta^\lambda \equiv \{\text{set of angles } \{\theta_i^\lambda\} \text{ defining } \mathscr{W}^h\} \tag{56}$$

and consider a square element $\Omega^e = (x_j, x_{j+1}) \times (y_j, y_{j+1})$ (Fig. 4). Denote by λ^{tb} the Lagrange multiplier on the top or bottom edge of the element ($y = y_{j+1}$ and $y = y_j$, respectively) and by λ^{lr} the Lagrange multiplier on the left or right edges of the element ($x = x_j$ and $x = x_{j+1}$, respectively). From (43) and (50), it follows that

$$\lambda^{tb} = \sum_{i=1}^{n^E} \lambda_i^{tb} \mathrm{e}^{((a_1 + |\mathbf{a}| \cos\theta_i)/2)(x - x_r^e)} \tag{57}$$

$$\lambda^{lr} = \sum_{i=1}^{n^E} \lambda_i^{lr} \mathrm{e}^{((a_2 + |\mathbf{a}| \sin\theta_i)/2)(y - y_r)} \tag{58}$$

where λ_i^{tb} and λ_i^{lr} are the unknown Lagrange multiplier dofs and the angles θ_i are those specified upon the selection of the enrichment basis.

In Eqs. (57) and (58), there is the possibility, depending on the set $\{\theta_i\}$, that $n^\lambda = n^E$, in which case condition (54) is not satisfied. Therefore, to ensure a non-singular global interface problem, the Lagrange multiplier discretizations (57) and (58) are next truncated

so that the recommended constraint (55) is satisfied. For a first order element having four or five enrichment functions like those considered in this work (Section 5), guideline (55) implies a single Lagrange multiplier per element edge. For such elements, Θ^λ is set to $\Theta^\lambda = \{\phi\}$ for a DGM element and $\Theta^\lambda = \{\phi - \pi\}$ for a true DEM element. The latter choice of θ^λ corresponds to a constant Lagrange multiplier per edge (see Remark 3).

Remark 5. For higher order elements, a systematic procedure or guideline is needed for selecting the set Θ^λ. Such a procedure is currently being developed and will be reported elsewhere.

5. Design of DGM and DEM rectangular elements for 2D advection–diffusion problems

The formulation of the enrichment functions u^E and Lagrange multipliers λ^h in terms of angle parameters θ_i is convenient. It enables the systematic design and implementation of DGM and DEM elements of arbitrary dimensions n^E, and their tailoring to the BVP of interest by rationally incorporating the direction ϕ implied by the advection coefficients a_1 and a_2. As suggested earlier, one strategy for selecting the angles defining the set Θ is to choose them so that the n^E enrichment functions they specify slope in n^E different directions. For instance for $n^E = 5$, this reasoning leads to the selection of the five basis functions graphically depicted in Fig. 3.

Next, a nomenclature is specified, some computational complexity issues are addressed, and several low order DGM and DEM elements are designed.

5.1. Notation and computational complexity

The rectangular DGM and DEM elements presented in this section are labeled as follows:

$$\text{DGM}: \ R - X - N$$

$$\text{DEM}: \ R - X - N^+ = [R - X - N] \cup [Q_1] \tag{59}$$

Here, R stands for rectangular, X is the number of enrichment functions n^E and N is the number of Lagrange multipliers per edge n^λ. The "+" superscript distinguishes a DEM element from a DGM element: in the former, the polynomial field of the Galerkin bilinear quadrilateral element Q_1 is included in the finite element basis so that $u^h = u^E + u^P$, whereas in the latter the polynomial field is omitted so that $u^h = u^E$. The computational complexity of several DGM and DEM elements is given in Table 3, assuming static condensation (Section 2.3) is implemented. In this table, n denotes the number of elements per direction, a square domain Ω as assumed in (49), and therefore the total number of elements is $n_{el} = n^2$. For reference, the computational complexity of each of the Galerkin Q_1 (bilinear) and Q_2 (biquadratic) polynomial elements is also given. Since the efficiency of an FEM depends not only on the total number of dofs but also the sparsity pattern of the resulting system matrix, Table 3 also reports the stencil width for an $n \times n$ uniform mesh. The reader can observe that the stencil of a DGM discretization is smaller than that of the Galerkin element that leads to a comparable total number of dofs for the given problem.

Remark 6. In Sections 2.4 and 4, it was shown that the cost of solving the matrix problem arising from the variational formulation (22) is not directly dependent on n^E but rather on the number of Lagrange multiplier dofs. Here, it is reminded however that there *is* a relationship between n^E and n^λ. The more enrichment functions are used, the more Lagrange multipliers are needed to enforce the inter-element continuity of the enriched solution. In practice, the relationship between X and N is given in Eq. (55).

Table 3
Computational complexity of some DGM, DEM and standard FEM elements

Element	Asymptotic # of dofs	Stencil width for uniform $n \times n$ mesh
Q_1	n^2	9
Q_2	$4n^2$	21
$R - X - 1$	$2n^2$	7
$R - X - 1^+$	$3n^2$	21

5.2. The $R - 4 - 1$ and $R - 5 - 1^+$ elements

The DGM element $R - 4 - 1$ and the true DEM element $R - 5 - 1^+$ are defined here by the sets Θ and Θ^λ specified below.

Element	Θ	Θ^λ
$R - 4 - 1$	$\phi, \phi + \frac{\pi}{2}, \phi - \frac{\pi}{2}, \phi - \pi$	ϕ
$R - 5 - 1^+$	$\phi, \phi + \frac{\pi}{2}, \phi - \frac{\pi}{2}, \phi + \frac{23\pi}{24}, \phi - \frac{23\pi}{24}$	$\phi - \pi$

Both elements have a single Lagrange multiplier per edge. The set of angles θ_i associated with each of these two elements are clustered "symmetrically" around the advection direction angle ϕ: for each chosen angle $\phi + \gamma_i$, the angle $\phi - \gamma_i$ is also chosen. Although such symmetry is not required, it avoids biasing the approximation to a specific orientation of the advection direction.

5.3. Element design for $Pe > 10^3$

An implementational difficulty arises when DEM is applied to a 2D advection–diffusion problem with a very high Péclet number ($Pe > 10^3$). A Péclet number of this magnitude or even higher can be encountered in high Reynolds number flows. In this case, it is found that even with the use of a reference point $\mathbf{x}_r^e$ inside each element Ω^e as in (44), for some choices of θ_i, the evaluation of some elements of the matrices $\mathbf{k}^{EE}$ and $\mathbf{k}^{EC}$ causes an overflow in finite precision arithmetic. The reason is that for certain values of θ_i, the coefficients inside the exponents of the exponentials can in this case become negative

$$a_1 + |\mathbf{a}| \cos\theta_i < 0 \quad \text{and/or} \quad a_2 + |\mathbf{a}| \sin\theta_i < 0 \tag{60}$$

Without loss of generality, suppose that $a_1 + |\mathbf{a}| \cos\theta_i < 0$ and $x_r^e > 0$. In this case,

$$e^{(a_1+|\mathbf{a}|\cos\theta_i/2)(x-x_r^e)} = e^{(a_1+|\mathbf{a}|\cos\theta_i/2)x} e^{-(a_1+|\mathbf{a}|\cos\theta_i/2)x_r^e} \gg e^{(a_1+|\mathbf{a}|\cos\theta_i/2)x} \tag{61}$$

because assumption (60) implies that

$$-\left(\frac{a_1 + |\mathbf{a}|\cos\theta_i}{2}\right) x_r^e \gg 0 \tag{62}$$

Thus, rather than decreasing the value of the enrichment function and preventing its evaluation from causing an overflow, the reference point drastically *increases* the already large value of the exponential enrichment function when scenario (60) occurs. In practice, this issue does not become a problem until $Pe > 10^3$. Unfortunately, the seemingly natural solution of using multiple reference points for dealing with this issue appears to cause the element matrices to become singular and therefore is not a viable remedy to the problem.

To remedy the above issue, the following approach is instead adopted in this work. For problems with $Pe > 10^3$, the advection coefficients used in the arguments of the exponential functions of the enrichment basis are limited to the value of 10^3. This upper limit value was experimentally determined to be safe. Designating by a bar the "advection-limited" coefficients, this leads to the approximation

$$\overline{u}^E(\mathbf{x};\phi)|_{\Omega^e} = \sum_{i=1}^{n^E} \mathrm{e}^{(\overline{a_1}+|\overline{\mathbf{a}}|\cos\theta_i/2)(x-x_r^e)} \mathrm{e}^{(\overline{a_2}+|\overline{\mathbf{a}}|\sin\theta_i/2)(y-y_r^e)} \tag{63}$$

where

$$\overline{a}_j = \min\{10^3, a_j\}, \quad j = 1,2 \tag{64}$$

Elements constructed using this approach are denoted by $\overline{R-X-N}$ and $\overline{R-X-N^+}$. In this case, it is noted that the basis functions (63) do *not* solve the homogeneous advection–diffusion equation *for the specified Péclet number*. Instead, they are free-space solutions of the homogeneous advection–diffusion equation for a *different* and lower Péclet number. Nevertheless, they are more related to the problem of interest than mere polynomials, and will be shown to outperform their standard Galerkin counterparts on most test problems considered in Section 6.

6. Numerical results

Here, the performance of the DGM and DEM elements proposed in this paper is assessed for three advection–diffusion (5) benchmark problems:

(i) A homogeneous problem whose solution happens to be spanned by the DGM basis (43).
(ii) A homogeneous problem whose solution is *not* spanned by the DGM basis (43).
(iii) A non-homogeneous BVP.

In each case, the performance of the DGM or DEM element is contrasted with that of a standard Galerkin element and several stabilized finite elements developed elsewhere. All comparisons are performed between elements of similar computational complexity *a priori*, either for a specified level of accuracy or for a fixed total number of dofs. It turns out that all comparisons are also performed between elements of similar convergence rate *a posteriori*.

For all three aforementioned test problems, the computational domain is the unit square $\Omega = (0,1)\times(0,1)$ uniformly discretized by an $n \times n$ mesh with $n_{el} = n^2$ elements. All reported errors are relative errors measured in the L^2 norm. For a DGM element with n^E enrichment functions, the L^2 error $\mathscr{E}$ is computed as follows:

$$\mathscr{E}^2 = \sum_e \left\| \sum_{i=1}^{n^E} d_i u^E(\mathbf{x};\theta_i)|_{\Omega^e} - u_{ex}(\mathbf{x})|_{\Omega^e} \right\|^2_{L^2(\Omega^e)} = \sum_e \left\{ \int_{\Omega^e} \left(\sum_{i=1}^{n^E} d_i u^E(\mathbf{x};\theta_i) - u_{ex} \right)^2 \mathrm{d}\Omega \right\} \tag{65}$$

where u_{ex} is the exact solution, $u^E(\mathbf{x};\theta_i)$ are the enrichment functions given by (43), and d_i are the enrichment dofs. All integrals and therefore all matrices and right hand sides in (23) are computed exactly.

Table 4
Homogeneous boundary layer problem of Section 6.1 with $Pe \leqslant 10^3$: relative L^2 errors (in %) for discretizations with approximately 400 dofs

Pe	ϕ/π	Q_1	STR	EST	FFH	$R-4-1$
10^2	0	8.97	7.62	7.62	8.59	3.06×10^{-13}
	1/6	1.31	1.14	1.15	1.25	1.18×10^{-14}
	1/5	1.31	–	–	–	3.44×10^{-13}
	1/4	1.31	1.14	1.15	1.26	2.66×10^{-13}
	1/3	1.31	–	–	–	3.12×10^{-13}
10^3	0	57.7	12.8	12.8	12.9	3.43×10^{-12}
	1/6	2.53	1.67	1.67	1.75	1.24×10^{-13}
	1/5	2.57	–	–	–	1.07×10^{-11}
	1/4	2.62	1.67	1.67	1.77	3.19×10^{-14}
	1/3	2.53	–	–	–	2.18×10^{-13}

6.1. Homogeneous boundary layer problem with a flow aligned with the advection direction

This first test problem is a restatement of the so-called "smooth boundary layer problem" discussed in [8, Section 5.1]. It is a homogeneous problem where Dirichlet boundary conditions are specified on the sides of $\Omega = (0,1)\times(0,1)$ so that the exact solution of the advection–diffusion problem is

$$u_{ex} = \frac{\mathrm{e}^{a_1(x-1)+a_2(y-1)} - 1}{\mathrm{e}^{-a_1-a_2} - 1} \tag{66}$$

Given that $l_\Omega = 1$ in (4) and $\kappa \equiv 1$, the global Péclet number in the domain Ω is

$$Pe = |\mathbf{a}| \tag{67}$$

Also since

$$a_1 = Pe\cos\phi, \quad a_2 = Pe\sin\phi \tag{68}$$

this test problem is conducted by specifying two parameters, Pe and the advection direction ϕ.

In [8, Section 5.1], Harari and co-workers report results for three different stabilized finite elements labeled as STR, EST and FFH. All three elements are stabilized versions of the bilinear quadrilateral Galerkin element Q_1. These elements differ in the way the stabilization parameter is computed. Five different advection directions, namely, $\phi = 0$, $\pi/6$ and $\pi/4$ (considered in [8]), and $\phi = \pi/5$ and $\pi/3$ (not considered in [8]) are considered here for three different element Péclet numbers, 2.5, 250 and 2.5×10^4. The corresponding global Péclet numbers on Ω are 10^2, 10^3 and 10^6, respectively.

From the expression of the exact solution (66) and the general form of the enrichment functions (43), it follows that $u_{ex} = u^E(\mathbf{x};\phi) + u^E(\mathbf{x};\phi-\pi)$.[3] Since for all elements designed in Section 5.2 $\{\phi, \phi-\pi\} \in \Theta$, the DGM or DEM solution of this problem can be expected to be exact up to machine precision.

Tables 4 and 5 report the relative errors in the solutions predicted by the Galerkin element Q_1, its three stabilized variants STR, EST and FFH, the DGM element $R-4-1$ for $Pe \leqslant 10^3$, and the "limited" DGM element $\overline{R-4-1}$ element for $Pe = 10^6$. In each case, n is chosen so that the discretization has approximately 400 dofs ($n = 20$ for elements Q_1, and $n = 14$ for elements $R-4-1$ and $\overline{R-4-1}$). For the two lower Péclet numbers, it is found that the solution computed using either of the considered DGM elements is continuous and exact to machine precision. Table 5 reports the advection-limited $\overline{R-4-1}$ element used for $Pe = 10^6$ outperforms the Galerkin element Q_1 by at least two orders of magnitude. This suggests that although the enrichment functions in the basis of that element are not free-space solutions of the considered advection–diffusion equation, they are

[3] Recall that $u^E(\mathbf{x};\phi-\pi) = \text{const}$ (see Remark 3).

Table 5
Homogeneous boundary layer problem of Section 6.1 with $Pe=10^6$: relative L^2 errors (in %) for discretizations with approximately 400 dofs

Pe	ϕ/π	Q_1	STR	EST	FFH	$\overline{R-4-1}$
10^6	0	8.44×10^4	12.9	12.9	12.9	2.24
	1/6	9.75×10^2	1.67	1.67	1.75	1.11×10^{-1}
	1/5	9.97×10^2	–	–	–	8.91×10^{-2}
	1/4	9.97×10^2	1.67	1.67	1.77	1.29×10^{-1}
	1/3	9.75×10^2	–	–	–	1.27×10^{-1}

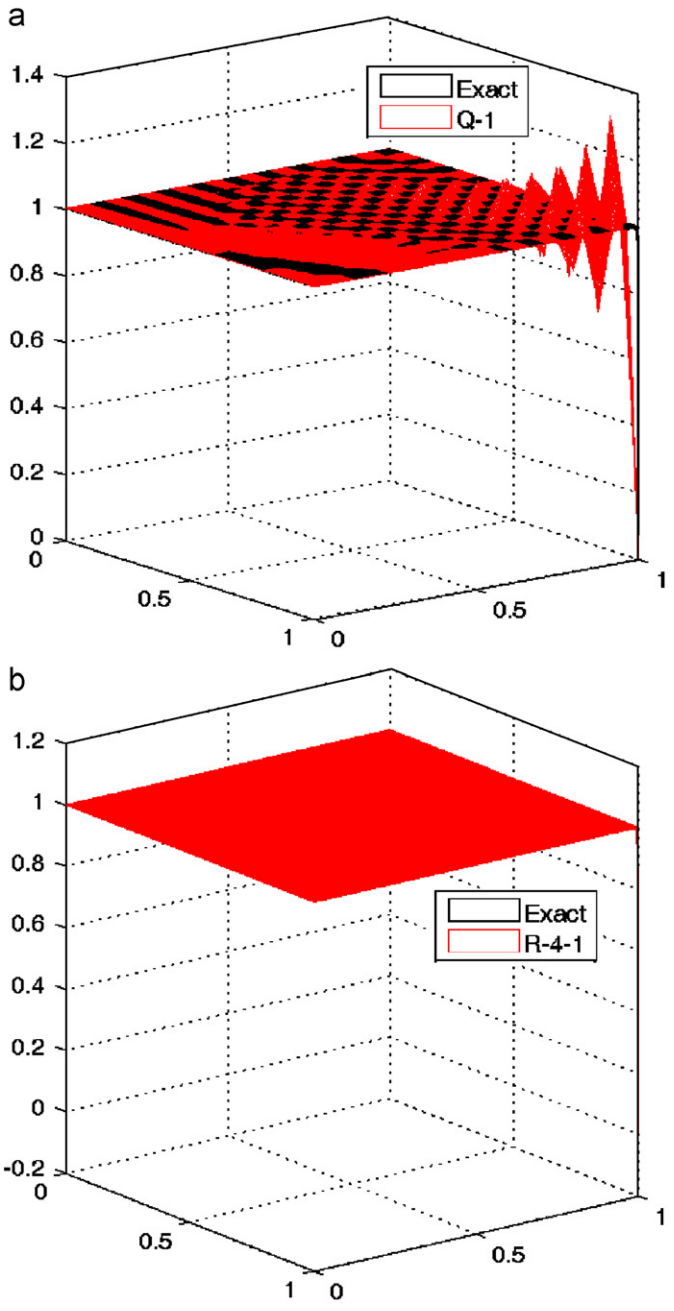

Fig. 5. Approximated and exact solutions of the homogeneous boundary layer problem of Section 6.1 with $\phi=\pi/6$ and $Pe=10^3$. (a) Q_1. (b) $R-4-1$.

still better at capturing the exact solution than the usual polynomial interpolants.

Fig. 5 compares the computed $R-4-1$ and Q_1 solutions with the exact solution when the advection direction is $\phi=\pi/6$ and $Pe=10^3$.

Table 6
Homogeneous boundary layer problem of Section 6.2 with $\phi=0$ and $Pe\leqslant10^3$: relative L^2 errors (in %) for discretizations with approximately 400 dofs

Pe	ψ/π	Q_1	$R-4-1$
1×10^2	0	8.97	3.06×10^{-13}
	1/4	1.26	1.70×10^{-1}
	1/2	1.07	1.19×10^{-1}
	3/4	1.05	8.18×10^{-1}
1×10^3	0	57.7	3.43×10^{-12}
	1/4	2.45	2.86×10^{-2}
	1/2	2.45	5.79×10^{-3}
	3/4	2.41	1.33×10^{-2}

Table 7
Homogeneous boundary layer problem of Section 6.2 with $\phi=0$ and $Pe=10^6$: relative L^2 errors (in %) for discretizations with approximately 400 dofs

Pe	ψ/π	Q_1	$\overline{R-4-1}$
1×10^6	0	8.44×10^4	2.24
	1/4	2.26×10^3	8.28×10^{-2}
	1/2	2.26×10^3	1.00×10^{-1}
	3/4	2.26×10^3	1.31×10^{-1}

The reader can observe that the DGM solution does not exhibit the spurious oscillations that pollute the Galerkin solution.

6.2. Homogeneous boundary layer problem with a flow not aligned with the advection direction

Next, the same problem as in Section 6.1 is considered but with different Dirichlet boundary conditions that are designed so that the exact solution of problem (5) is

$$u_{ex}=\frac{e^{Pe/2(\cos\phi+\cos\psi)(x-1)+Pe/2(\sin\phi+\sin\psi)(y-1)}-1}{e^{-Pe/2(\cos\phi+\sin\psi+\sin\phi+\cos\psi)}-1} \tag{69}$$

where $\phi\in[0,2\pi)$ is the advection–direction implied by the advection coefficients a_1 and a_2 in (5) and $\psi\in[0,2\pi)$ is some flow direction. Here, it is emphasized that solutions of the form in (69) are *not* in general in the span of $\mathcal{V}^E$ given by (43), except for certain values of ϕ and ψ, e.g., $\phi=\psi=0$.

The advection direction is fixed to $\phi=0$ and ψ is varied between 0 and π. The same elements as before are considered and in all cases the size of the discretization is fixed to roughly 400 dofs ($n=14$ for elements $R-4-1$ and $\overline{R-4-1}$; $n=20$ for elements Q_1). (Note that when $\phi=\psi=0$, the exact solutions (69) and (66) are identical and well captured by the DGM elements).

The performance results reported in Tables 6 and 7 show that for $\psi\neq0$, the relative errors associated with the DGM solutions are several orders of magnitude lower than those associated with the standard Galerkin solutions. This illustrates how the enrichment functions in each of the bases of the $R-4-1$ and $\overline{R-4-1}$ elements successfully combine to efficiently capture the exact solution (69) which is *not* represented in either of these two bases. In particular, the reader can observe the excellent performance of the $\overline{R-4-1}$ element at $Pe=10^6$ despite the fact that this element's basis functions are *not* free-space solutions of the advection–diffusion equation for $Pe=10^6$ (see Table 7 and Fig. 6).

Table 8 reports for this problem the convergence rates measured in the L^2 norm for both the standard Galerkin element Q_1 and the DGM element $R-4-1$, when the mesh size is increasingly refined (see Fig. 7). Both elements deliver in this metric a quadratic convergence rate. Hence, these two elements are called here "comparable" from this viewpoint. However, Fig. 7 clearly shows that for a fixed mesh

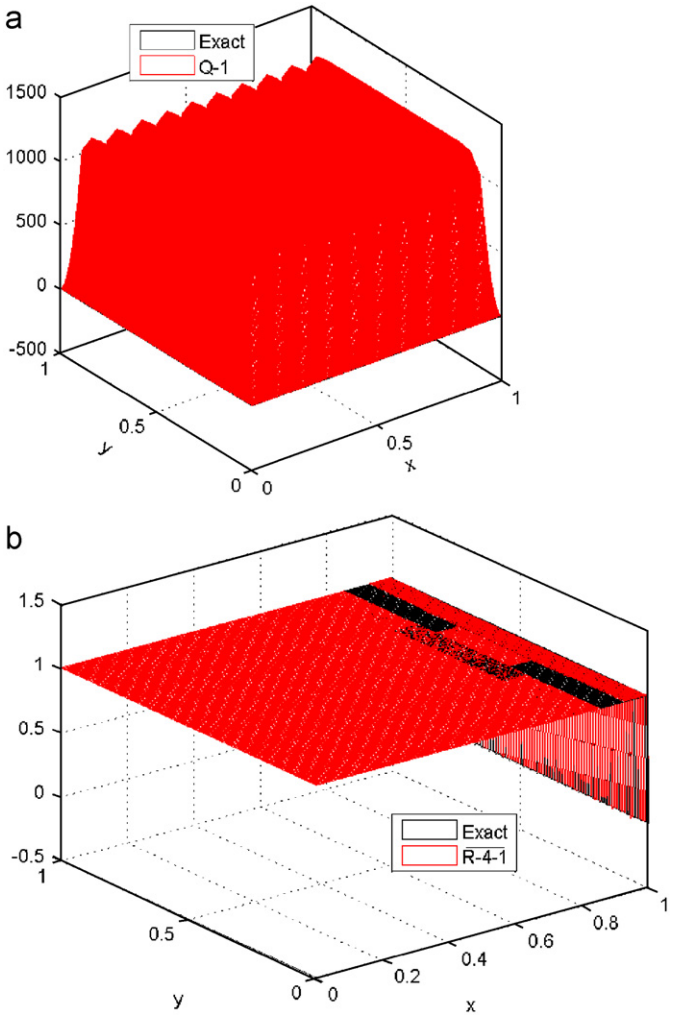

Fig. 6. Approximated and exact solutions of the homogeneous boundary layer problem of Section 6.2 with $\phi = \psi = 0$ and $Pe = 10^6$. (a) Q_1. (b) $\overline{R-4-1}$.

Table 8
Convergence rates measured in the L^2 norm for the homogeneous boundary layer problem of Section 6.2 with $\phi = 0$, $\psi = \pi/4$ and $Pe = 10^2$

Element	Convergence rate
Q_1	1.8461
$R-4-1$	1.8901

size, the solution delivered by the DGM element $R-4-1$ is an order of magnitude more accurate than that delivered by the standard Q_1 element.

6.3. Two-scale non-homogeneous problem

To highlight the role of the polynomial field u^P in DEM, a non-homogeneous variant of the boundary layer problem defined in Section 6.1 is considered here. More specifically, the source term

$$f(x,y) = 2(a_1 x + a_2 y - 2) \tag{70}$$

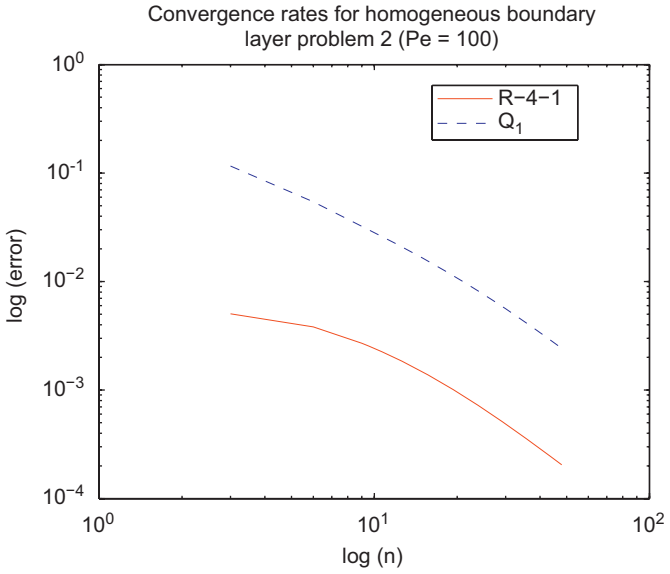

Fig. 7. Convergence histories measured in the L^2 norm for the homogeneous boundary layer problem of Section 6.2 with $\phi = 0$, $\psi = \pi/4$ and $Pe = 10^2$.

Table 9
Non-homogeneous boundary layer problem of Section 6.3 with $Pe \leqslant 10^3$: relative L^2 errors (in %) for discretizations with approximately 1600 dofs

Pe	ϕ/π	Q_1	$R-5-1^+$
10^2	0	4.05	7.68×10^{-5}
	1/6	5.27×10^{-1}	2.72×10^{-5}
	1/5	5.20×10^{-1}	2.77×10^{-5}
	1/4	5.17×10^{-1}	2.77×10^{-5}
	1/3	5.27×10^{-1}	2.72×10^{-5}
10^3	0	22.4	3.94×10^{-4}
	1/6	1.34	1.39×10^{-4}
	1/5	1.35	1.20×10^{-4}
	1/4	1.36	9.75×10^{-5}
	1/3	1.34	1.39×10^{-4}

Table 10
Non-homogeneous boundary layer problem of Section 6.3 with $Pe = 10^6$: relative L^2 errors (in %) for discretizations with approximately 1600 dofs

Pe	ϕ/π	Q_1	$\overline{R-5-1^+}$
10^6	0	2.75×10^4	3.60
	1/6	1.55×10^2	6.70
	1/5	1.58×10^2	6.83
	1/4	5.45×10^2	5.63
	1/3	1.56×10^2	4.47

is added and the Dirichlet boundary conditions are designed so that the exact solution to problem (5) is now

$$u_{ex} = \underbrace{x^2 + y^2}_{\text{slowly varying}} + \underbrace{\left(\frac{e^{a_1(x-1)+a_2(y-1)} - e^{-a_1-a_2}}{e^{-a_1-a_2} - 1} \right)}_{\text{rapidly varying}} \tag{71}$$

This exact solution contains two scales: a rapidly varying exponential *and* a slowly varying polynomial. Because of this multi-scale behavior, a true DEM element whose approximation basis includes the enrichment as well as the polynomial field ($u^h = u^P + u^E$) is used to solve this problem. Tables 9 and 10 report the obtained performance results for the DEM element $R-5-1^+$ for $Pe \leqslant 10^3$ and the DEM element $\overline{R-5-1^+}$ for $Pe=10^6$, respectively, and contrast them with the performance of the Q_1 element when the size of the discretization

Table 11
Convergence rates measured in the L^2 norm for the non-homogeneous boundary layer problem of Section 6.3 with $\phi = 0$ and $Pe = 10^2$

Element	Convergence rate
Q_1	1.6919
$R-5-1^+$	2.0789

is fixed around approximately 1600 dofs ($n = 40$ for the Q_1 element and $n = 24$ for the $R-5-1^+$ and $\overline{R-5-1^+}$ elements).

Tables 9 and 10 report that the DEM elements outperform the Galerkin element by several orders of magnitude. The achieved relative errors are not quite as low as those reported in Tables 4 and 5 for the homogeneous problem of Section 6.1 because the finite element bases of the DEM elements do not contain in this case the exact solution (71) given that the polynomial field u^P of Q_1 is bilinear and *not* biquadratic. Nonetheless, the magnitudes of these achieved relative errors reveal that the $R-5-1^+$ DEM element successfully captures both the fine or rapidly varying and the coarse or slowly varying scales of the solution for $Pe \leqslant 10^3$.

Table 10 reports that even the advection-limited DEM element $\overline{R-5-1^+}$ used to solve the problem at $Pe = 10^6$ performs quite well relatively to the Galerkin element Q_1. Table 11 reports that the DEM element $R-5-1^+$ converges quadratically with respect to the mesh size in the L^2 norm, and therefore is comparable to the standard Galerkin element Q_1 in convergence rate, but has a dramatically lower error constant.

Perhaps more illustrative than the errors reported in Tables 9 and 10 are the plots of the computed solutions displayed in Fig. 8. Whereas the Q_1 solution is shown to exhibit spurious oscillations, the DEM solution is shown to be virtually indistinguishable from the exact solution in the entire computational domain.

7. Conclusions

In the discontinuous enrichment method (DEM) first proposed in [13], the standard finite element polynomials are enriched within each element by discontinuous functions that are chosen as the free-space solutions of the homogeneous, constant-coefficient version of the governing PDE and Lagrange multiplier degrees of freedom (dofs) are introduced at the element boundaries to enforce a weak continuity of the solution. The free-space solution nature of the enrichment field enables the exact computation of the element level matrices, and the discontinuous nature of the approximation enables the static condensation of the enrichment dofs prior to the assembly of these matrices. Overall, the computational complexity of DEM is dictated by the total number of Lagrange multiplier dofs, the number of polynomial dofs and the sparsity pattern of the corresponding system matrix.

In this paper, DEM was developed for the two-dimensional advection–diffusion equation. The enrichment field was derived for this equation and found to include a set of exponential functions, each exhibiting a sharp gradient in some direction $\theta_i \in [0, 2\pi)$. These functions have been used in the finite element approximation space either on their own (DGM element) in the case of homogeneous BVPs, or in conjunction with the standard Galerkin polynomial field u^P in the case of non-homogeneous BVPs (true DEM elements). The advection–diffusion basis presented in this paper is nicely parameterized in a manner that provides a systematic procedure for designing DGM and DEM elements of arbitrary orders. For $Pe \leqslant 10^3$, two first order, rectangular elements each with one Lagrange multiplier per edge have been designed and labeled $R-4-1$ (DGM elements) and $R-5-1^+$ (DEM element). For $Pe > 10^3$, a special class of advection-limited version of these elements has also been constructed. The performance of these DGM and DEM elements

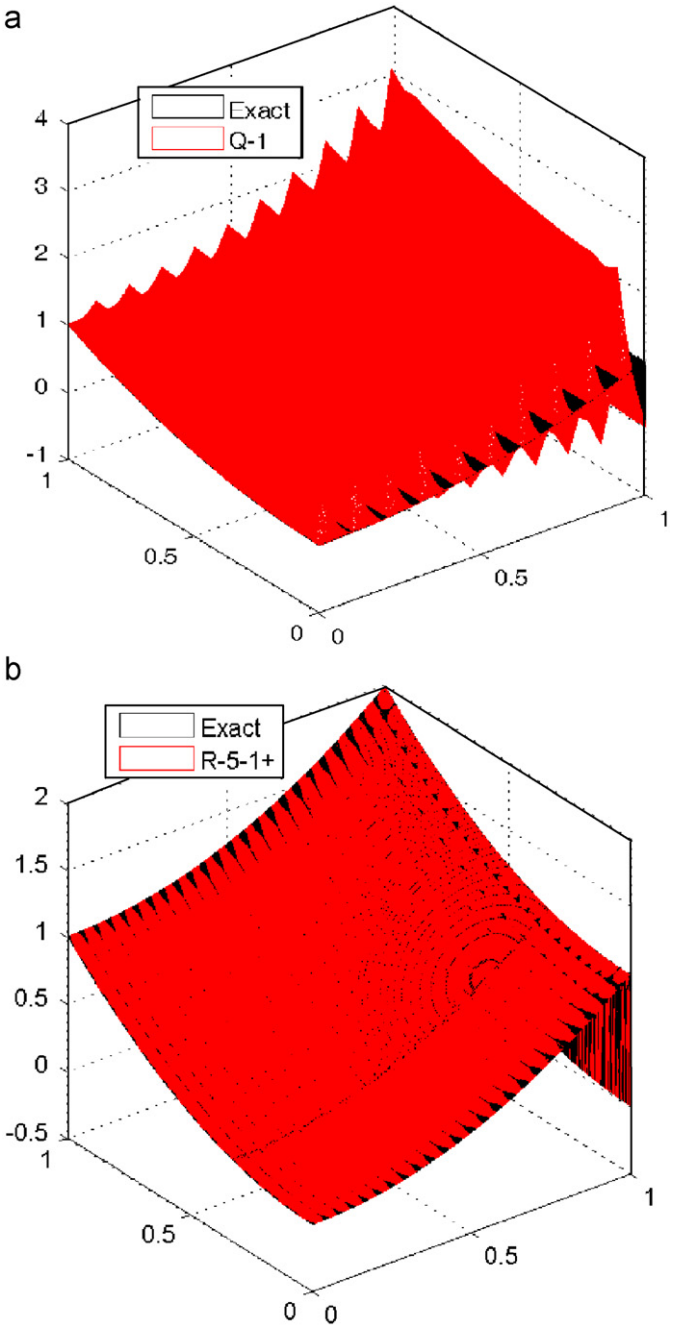

Fig. 8. Approximated and exact solutions of the non-homogeneous boundary layer problem of Section 6.3 with $\phi = 0$ and $Pe = 10^3$. (a) Q_1. (b) $R-5-1^+$.

was assessed for three benchmark problems, two of which were previously studied in the literature. In all cases, the DGM and DEM elements demonstrated an impressive performance. In particular, they outperformed standard Galerkin and stabilized finite elements of comparable complexity and comparable order of convergence by a large margin, thereby demonstrating a serious potential for realistic transport problems at high Péclet number.

Acknowledgments

The first author acknowledges the support by an NDSEG Fellowship sponsored by the U.S. Department of Defense. The second and third authors acknowledge the support by the Office of Naval Research under Grant N00014-08-1-0184.

References

[1] A.N. Brooks, T.J.R. Hughes, Streamline upwind/Petrov–Galerkin formulations for convection dominated flows with particular emphasis on the incompressible Navier–Stokes equations, Comput. Math. Appl. Mech. Eng. 32 (1982) 199–259.

[2] T.J.R. Hughes, A.N. Brooks, A multi-dimensional upwind scheme with no crosswind diffusion, in: T.J.R. Hughes (Ed.), Finite Element Methods for Convection Dominated Flows, Applied Mechanics Division (AMD), American Society of Mechanical Engineers, vol. 34, 1979, pp. 19–35.

[3] I. Harari, T.J.R. Hughes, Galerkin/least squares finite element methods for the reduced wave equation with non-reflecting boundary conditions in unbounded domains, Comput. Methods Appl. Mech. Eng. 98 (1992) 411–454.

[4] T.J.R. Hughes, L.P. Franca, G.M. Hulbert, A new finite element formulation for computational fluid dynamics: VIII. The Galerkin/least-squares method for advective–diffusive equations, Comput. Methods Appl. Mech. Eng. 73 (2) (1989) 173–189.

[5] L.P. Franca, S.L. Frey, T.J.R. Hughes, Stabilized finite element methods, I. Application to the advective–diffusive model, Comput. Methods Appl. Mech. Eng. 95 (1992) 253–276.

[6] L.P. Franca, C. Farhat, Bubble functions prompt unusual stabilized finite element methods, Comput. Methods Appl. Mech. Eng. 123 (1995) 299–308.

[7] R. Araya, E. Behrens, R. Rodriguez, An adaptive stabilized finite element scheme for the advection–reaction–diffusion equation, Appl. Numer. Math. 54 (2005) 491–503.

[8] I. Harari, L.P. Franca, S.P. Oliveira, Streamline design of stability parameters for advection–diffusion problems, J. Comput. Phys. 171 (2001) 115–131.

[9] F. Brezzi, A. Russo, Choosing bubbles for advection–diffusion problems, Math. Models Methods Appl. Sci. 4 (4) (1994) 571–587.

[10] F. Brezzi, D. Marini, A. Russo, Applications of the pseudo residual-free bubbles to the stabilization of convection–diffusion problems, Comput. Methods Appl. Mech. Eng. 166 (1998) 51–63.

[11] I. Babuška, J.M. Melenk, The partition of unity method, Int. J. Numer. Methods Eng. 40 (1997) 727–758.

[12] J.M. Melenk, I. Babuška, The partition of unity method finite element method: basic theory and applications, Comput. Methods Appl. Mech. Eng. 139 (1996) 289–314.

[13] C. Farhat, I. Harari, L.P. Franca, The discontinuous enrichment method, Comput. Methods Appl. Mech. Eng. 190 (2001) 6455–6479.

[14] C. Farhat, I. Harari, U. Hetmaniuk, A discontinuous Galerkin method with Lagrange multipliers for the solution of Helmholtz problems in the mid-frequency regime, Comput. Methods Appl. Mech. Eng. 192 (2003) 1389–1419.

[15] R. Tezaur, C. Farhat, Three-dimensional discontinuous Galerkin elements with plane waves and Lagrange multipliers for the solution of mid-frequency Helmholtz problems, Int. J. Numer. Methods Eng. 66 (2006) 796–815.

[16] R. Tezaur, L. Zhang, C. Farhat, A discontinuous enrichment method for capturing evanescent waves in multi-scale fluid and fluid/solid problems, Comput. Methods Appl. Mech. Eng., 2007, in press.

[17] L. Zhang, R. Tezaur, C. Farhat, The discontinuous enrichment method for elastic wave propagation in the medium-frequency regime, Int. J. Numer. Methods Eng. 66 (2006) 2086–2114.

[18] I. Babuška, C.E. Baumann, J.T. Oden, A discontinuous HP finite element method for diffusion problems: 1-D analysis, Comput. Math. Appl. 37 (1999) 103–122.

[19] C.E. Baumann, J.T. Oden, A discontinuous HP finite element method for the Euler and Navier–Stokes equations, Int. J. Numer. Methods Fluids 31 (1999) 79–96 (Tenth International Conference on Finite Elements in Fluids, Tucson, AZ, 1998).

[20] A. El-Zein, Exponential finite elements for diffusion–advection problems, Int. J. Numer. Methods Eng. 62 (2005) 2086–2103.

[21] E.H. Georgoulis, E. Hall, P. Houston, Discontinuous Galerkin methods for advection–diffusion–reaction problems on anisotropically refined meshes, SIAM J. Sci. Comput. 30 (1) (2007) 246–271.

[22] F. Brezzi, M. Fortin, Mixed and Hybrid Finite Element Methods, Springer, New York, NY, 1991.